On passivity-based trajectory tracking for robotic manipulators combining PD+ and Slotine-Li control

Lakatos, Kristin; Lakatos, Dominic; Wu, Xuwei; Kotyczka, Paul; Dietrich, Alexander

Research Article

Kristin Lakatos*, Dominic Lakatos, Xuwei Wu, Paul Kotyczka, and Alexander Dietrich

On passivity-based trajectory tracking for robotic manipulators combining PD+ and Slotine-Li control

Zur passivitätsbasierten Trajektorienfolgeregelung für Roboterarme, die PD+ und Slotine-Li Regelung kombiniert

https://doi.org/10.1515/sample-YYYY-XXXX
Received Month DD, YYYY; revised Month DD, YYYY; accepted Month DD, YYYY

Abstract: In this paper, a tracking controller for robots is analyzed, which allows both the specification of the convergence rate of the tracking errors and the parameterization of a desired contact stiffness and damping. It is shown that the control approach can be interpreted as a generalization of the well-known PD+ and Slotine-Li controllers, combining the benefits of both approaches. Although mentioned in the literature before, no thorough theoretical and practical analysis of the aforementioned passivity-based control concept has been performed so far. In this work, the implications of the gains are discussed w. r. t. convergence and interaction properties, addressing possible tuning strategies. Finally, the performance of the controller is evaluated in terms of tracking and interaction experiments on a KUKA LWR IV+.

Keywords: Robot control, trajectory tracking, passivity-based control, human-robot interaction

Zusammenfassung: In dieser Arbeit wird ein Trajektorienfolgeregler für Roboterarme analysiert. Dieser erlaubt sowohl die Spezifikation einer Konvergenzrate für die Regelfehler als auch die Parametrisierung einer gewünschten Kontaktsteifigkeit und Dämpfung. Es wird gezeigt, dass der Regler als eine Verallgemeinerung der bekannten PD+ und Slotine-Li-Regler interpretiert werden kann und dabei die Vorteile beider Ansätze vereint. Obwohl das besagte passivitätsbasierte Regelgesetz in der Literatur bereits bekannt ist, wurde bisher noch keine umfassende Analyse der theoretischen und praktischen Eigenschaften veröffentlicht. In dieser Arbeit wird daher insbesondere die Bedeutung der Verstärkungsfaktoren hinsichtlich der Konvergenz- und Interaktionseigenschaften diskutiert. Dabei werden verschiedene Gain-Tuning-Strategien aufgezeigt. Die Performanz des Reglers wird schließlich anhand von Trajektorienfolge und Mensch-Roboter-Interaktions-Experimenten an einem KUKA LWR IV+ Roboterarm evaluiert.

Schlagwörter: Roboterregelung, Trajektorienfolgeregelung, passivitätsbasierte Regelung, Mensch-Roboter Interaktion

1 Introduction

Trajectory tracking control of robotic manipulators has been a topic of interest for many decades, especially regarding the use of robots in industrial applications. In this context, the tracking performance as well as convergence rates are crucial indicators for the choice of a well-suited control algorithm. Moreover, the capability to specify the behavior in contact with the environment becomes more and more important, particularly in scenarios with human-robot collaboration.

Classical approaches for trajectory tracking include among others feedback-linearizing algorithms such as *inverse dynamics* or *computed torque control* schemes [1, 2]. These methods yield linear closed-loop dynamics, potentially at the cost of robustness issues in the presence of modeling uncertainties and external disturbances [3]. To overcome these drawbacks, an additional class of control algorithms for trajectory tracking has been developed in the

***Corresponding author: Kristin Lakatos,** Institute of Robotics and Mechatronics, German Aerospace Center (DLR). Contact: kristin.lakatos@dlr.de
Dominic Lakatos, Xuwei Wu, Alexander Dietrich, Institute of Robotics and Mechatronics, German Aerospace Center (DLR).
Paul Kotyczka, Technical University of Munich, TUM School of Engineering and Design, Department of Engineering Physics and Computation.

1980s. These controllers exploit inherent physical properties of the robot dynamics. They are based on the concept of preserving passivity by shaping the energy of the closed-loop system and thus are referred to as *passivity-based control* [4, 5, 6]. Nowadays, these control algorithms are widely used, since they are robust w. r. t. disturbances and modeling uncertainties[1]. The historical and practical importance of passivity-based control concepts is highlighted among others in [7, 8]. One of the fundamental tracking controllers for robots is the PD+ controller, that has been introduced by Paden and Panja in [4]. It allows to specify a desired stiffness and damping behavior. However, the stability analysis is limited to qualitative statements about the convergence of the control error. An alternative approach for tracking control has been presented in the seminal work of Slotine and Li [5, 9, 10]. In contrast to the PD+ controller, the Slotine-Li controller (SLC) allows a direct parameterization of the convergence rate. This, however, determines the contact stiffness and damping.

The focus of this work is a control algorithm which combines the advantages of both PD+ control and SLC. As the control law can be interpreted as a generalization of the PD+ controller and the SLC, we will refer to it as *Generalized Robot Tracking Controller (GTC)*. On the one hand, it allows to set the contact stiffness, while quantitative statements about the convergence rate can still be made. On the other hand, the convergence rate can be specified directly. In that case, it is still possible to influence the effective stiffness by weighting the gains accordingly. The control law at hand has already been introduced in [6], where exponential stability has been proven based on a Lyapunov function. In [11], [12], and [13], the control law is applied in the context of velocity observer design, disturbance attenuation, and omnidirectional mobile platforms, respectively. Still, to the best of our knowledge, no thorough analysis of the GTC control law – especially in comparison to PD+ control and SLC – has been performed so far. This work reviews the GTC and further analyzes it from an application perspective. The theoretical as well as the practical advantages compared to the pure PD+ and SLC approaches are shown. Regarding the increasing importance of human-robot collaboration in the industry, the analyses in this work focus particularly on the contact properties of the controller. This aspect of the GTC has not been considered in the literature so far. Thus, the contributions of this work include

- the analysis of the GTC as a generic case containing both PD+ control and SLC,
- an extension of the GTC to task space trajectory tracking,
- the presentation of a novel proof of stability, which allows a reduction of the effective stiffness w. r. t. a pure SLC implementation,
- discussions on the implications of the gain design w. r. t. tracking and interaction properties,
- a proposition of possible tuning strategies for the GTC,
- a performance evaluation of the tracking controller, using experiments on a commercial industrial robot, the KUKA LWR IV+.

The theoretical and experimental results reveal that it is possible to significantly reduce the perceived stiffness compared to a baseline SLC implementation while maintaining the full tracking performance on velocity level. Additionally, it is shown that the tracking performance of the SLC implementation can be improved by increasing the stiffness gain based on the control law at hand. Note that both SLC and GTC are originally introduced together with a parameter adaption part. However, we omit this parameter adaption for the sake of clarity and comparability, assuming perfect knowledge of the system model.

The paper is organized as follows: The system model and problem statement are given in Sec. 2. In Sec. 3.1, the generalized robot tracking controller is described. A discussion of its properties follows in Sec. 3.2, an extension to task-space control is proposed in Sec. 3.3. In Sec. 4, experimental results are shown. In Sec. 5, the findings of this work are discussed. Sec. 6 concludes the paper.

2 System model

A serial robotic arm with n joint coordinates $\boldsymbol{q} \in \mathcal{Q} \subset \mathbb{R}^n$ can be modeled by the second-order rigid-body dynamics equations[2]

$$\boldsymbol{M}(\boldsymbol{q})\ddot{\boldsymbol{q}} + \boldsymbol{C}(\boldsymbol{q}, \dot{\boldsymbol{q}})\dot{\boldsymbol{q}} + \boldsymbol{g}(\boldsymbol{q}) = \boldsymbol{\tau} + \boldsymbol{\tau}_{\text{ext}}. \tag{1}$$

1 This means that the mentioned passivity-based control approaches cannot be destabilized by certain unmodeled effects like joint friction. In comparison, control approaches laws using feedback linearization techniques can indeed be destabilized, which is theoretically discussed and practically shown e. g. in [3].

2 Geometrically, the (unconstrained) configuration manifold $\mathcal{M}$ of an n-link revolute joint serial robot is the n-torus $(\mathcal{S}^1)^n$. We parameterize $(\mathcal{S}^1)^n$ through the minimal joint coordinates $(q_1, \ldots, q_n) \in \mathcal{Q} \subset \mathbb{R}^n$, where $\mathcal{Q}$ describes the admissible joint angles in a subset of $[-\pi, \pi)$ each, given by the operation limits of the robot. We therefore perform trajectory tracking and stability analysis in a subspace of Euclidean space.

The following well-known properties hold:

1. The inertia matrix $\boldsymbol{M}(\boldsymbol{q}) \in \mathbb{R}^{n\times n}$ is symmetric positive definite (also written as s.p.d. or $\boldsymbol{M} \succ \boldsymbol{0}$) [14, p.171] and uniformly bounded [15].
2. The effect of Coriolis/centrifugal forces is modeled by $\boldsymbol{C}(\boldsymbol{q},\dot{\boldsymbol{q}})\dot{\boldsymbol{q}}$ with $\boldsymbol{C} \in \mathbb{R}^{n\times n}$, such that $\dot{\boldsymbol{M}} - 2\boldsymbol{C}$ is skew-symmetric [14, p.171].

Gravitational forces are written as $\boldsymbol{g}(\boldsymbol{q}) \in \mathbb{R}^n$. The considered robot features a torque interface in each joint and is assumed to be fully actuated through $\boldsymbol{\tau} \in \mathbb{R}^n$. External torques are denoted by $\boldsymbol{\tau}_{\text{ext}} \in \mathbb{R}^n$.

A desired, time-dependent trajectory in the joint space is given by $\boldsymbol{q}_{\text{des}}(t), \dot{\boldsymbol{q}}_{\text{des}}(t), \ddot{\boldsymbol{q}}_{\text{des}}(t)$. It is assumed to be continuous in time and feasible. Moreover, all desired joint positions, velocities, and accelerations are assumed to be bounded. The corresponding tracking error is defined as

$$\widetilde{\boldsymbol{q}}(t) = \boldsymbol{q} - \boldsymbol{q}_{\text{des}}(t) \tag{2}$$

with the time derivatives $\dot{\widetilde{\boldsymbol{q}}}(t), \ddot{\widetilde{\boldsymbol{q}}}(t)$. In the following, time dependencies are only written where strictly necessary for the understanding.

3 Passivity-based robot tracking control

In this section, the GTC as a unifying passivity-based tracking controller for (1) is discussed with reference to two standard tracking controllers in robotics. For the sake of comparison and discussion, both the PD+ controller [4] as well as the SLC [5] with some relevant properties will be recapitulated in the following.

PD+ controller [4]: The control law is

$$\begin{aligned}\boldsymbol{\tau}_{\text{PD+}} = \boldsymbol{M}(\boldsymbol{q})\ddot{\boldsymbol{q}}_{\text{des}} + \boldsymbol{C}(\boldsymbol{q},\dot{\boldsymbol{q}})\dot{\boldsymbol{q}}_{\text{des}} + \boldsymbol{g}(\boldsymbol{q}) - \\ -\boldsymbol{K}\widetilde{\boldsymbol{q}} - \boldsymbol{D}(\boldsymbol{q})\dot{\widetilde{\boldsymbol{q}}}\end{aligned} \tag{3}$$

with $\boldsymbol{K} \in \mathbb{R}^{n\times n}$ and $\boldsymbol{D}(\boldsymbol{q}) \in \mathbb{R}^{n\times n}$ being s.p.d. gain matrices. Applying (3) to (1), the closed-loop dynamics become

$$\boldsymbol{M}(\widetilde{\boldsymbol{q}},t)\ddot{\widetilde{\boldsymbol{q}}} + (\boldsymbol{C}(\widetilde{\boldsymbol{q}},\dot{\widetilde{\boldsymbol{q}}},t) + \boldsymbol{D}(\widetilde{\boldsymbol{q}},t))\dot{\widetilde{\boldsymbol{q}}} + \boldsymbol{K}\widetilde{\boldsymbol{q}} = \boldsymbol{\tau}_{\text{ext}}. \tag{4}$$

It is, with some intermediate considerations, possible to show uniform exponential stability of $(\widetilde{\boldsymbol{q}}^*, \dot{\widetilde{\boldsymbol{q}}}^*) = (\boldsymbol{0},\boldsymbol{0})$ for the undisturbed system ($\boldsymbol{\tau}_{\text{ext}} = \boldsymbol{0}$) with the Lyapunov function

$$\begin{aligned}V_{\text{PD+}}(\widetilde{\boldsymbol{q}},\dot{\widetilde{\boldsymbol{q}}},t) = \frac{1}{2}\dot{\widetilde{\boldsymbol{q}}}^T\boldsymbol{M}(\widetilde{\boldsymbol{q}},t)\dot{\widetilde{\boldsymbol{q}}} + \frac{1}{2}\widetilde{\boldsymbol{q}}^T\boldsymbol{K}\widetilde{\boldsymbol{q}} + \\ + \epsilon\dot{\widetilde{\boldsymbol{q}}}^T\boldsymbol{M}(\widetilde{\boldsymbol{q}},t)\widetilde{\boldsymbol{q}}\end{aligned} \tag{5}$$

with a sufficiently small positive constant ϵ (see e. g. [14, p. 194-195]). One major advantage of the use of a PD+ controller is the direct realization of a desired contact stiffness and damping through $\boldsymbol{K}$ and $\boldsymbol{D}(\boldsymbol{q})$, respectively[3].

Slotine-Li controller [5]: The control law (assuming no parameter uncertainties) is given as

$$\boldsymbol{\tau}_{\text{SLC}} = \boldsymbol{M}(\boldsymbol{q})\ddot{\boldsymbol{q}}_{\text{ref}} + \boldsymbol{C}(\boldsymbol{q},\dot{\boldsymbol{q}})\dot{\boldsymbol{q}}_{\text{ref}} + \boldsymbol{g}(\boldsymbol{q}) - \boldsymbol{H}(\boldsymbol{q})\boldsymbol{s}. \tag{6}$$

with a s.p.d. gain matrix $\boldsymbol{H}(\boldsymbol{q}) \in \mathbb{R}^{n\times n}$. Thereby, the *reference trajectory* is constructed as a combination of the desired velocities with weighted position errors

$$\dot{\boldsymbol{q}}_{\text{ref}} = \dot{\boldsymbol{q}}_{\text{des}} - \boldsymbol{\Omega}\widetilde{\boldsymbol{q}}, \tag{7}$$

with a diagonal p.d. matrix $\boldsymbol{\Omega} \in \mathbb{R}^{n\times n}$. The so-called *sliding variable* is defined as

$$\boldsymbol{s} = \dot{\boldsymbol{q}} - \dot{\boldsymbol{q}}_{\text{ref}} = \dot{\widetilde{\boldsymbol{q}}} + \boldsymbol{\Omega}\widetilde{\boldsymbol{q}}. \tag{8}$$

Then, the closed-loop dynamic equations become

$$\boldsymbol{M}(\widetilde{\boldsymbol{q}},t)\dot{\boldsymbol{s}} + (\boldsymbol{C}(\widetilde{\boldsymbol{q}},\boldsymbol{s},t) + \boldsymbol{H}(\widetilde{\boldsymbol{q}},t))\boldsymbol{s} = \boldsymbol{\tau}_{\text{ext}} \tag{9}$$

$$\dot{\widetilde{\boldsymbol{q}}} = \boldsymbol{s} - \boldsymbol{\Omega}\widetilde{\boldsymbol{q}}. \tag{10}$$

In [16], uniform exponential stability of the origin $(\widetilde{\boldsymbol{q}}^*, \boldsymbol{s}^*) = (\boldsymbol{0},\boldsymbol{0})$ for the undisturbed system is shown with the Lyapunov function

$$V_{\text{SLC}}(\widetilde{\boldsymbol{q}},\boldsymbol{s},t) = \frac{1}{2}\boldsymbol{s}^T\boldsymbol{M}(\widetilde{\boldsymbol{q}},t)\boldsymbol{s} + \widetilde{\boldsymbol{q}}^T\boldsymbol{\Omega}\boldsymbol{H}\widetilde{\boldsymbol{q}}, \tag{11}$$

under the additional assumption that $\boldsymbol{H}$ is constant and diagonal. Using (11) as storage function, it is also possible to directly show passivity with input $\boldsymbol{\tau}_{\text{ext}}$ and output $\boldsymbol{s}$. In contrast to the PD+ controller, the convergence of the error and the error rate can directly be specified through $\boldsymbol{H}$ and $\boldsymbol{\Omega}$. On the other hand, it is not possible to assign decoupled physical stiffness and damping properties via an appropriate choice of the gains.

3.1 Generalized robot tracking controller

Some theoretical and practical drawbacks arise from the use of PD+ controller and SLC. The most obvious is that for both control laws, the stability analysis uses Lyapunov functions which are not directly related to the physical energy of the system. Thus, computing the convergence

3 Typically, $\boldsymbol{K}$ is chosen diagonal and constant in joint space tracking control, whereas the damping matrix $\boldsymbol{D}(\boldsymbol{q})$ might be configuration-dependent.

rate of the tracking errors does not necessarily give information about the decay of potential and kinetic energy of the robot. Also, tuning the gains is restricted to either influencing contact properties directly (PD+) or tuning the pure tracking performance (SLC).

To address the aforementioned disadvantages, the generalized robot tracking controller will be reviewed in the following. It features the following beneficial properties:

a) Uniform exponential stability with a more physically motivated Lyapunov function than for PD+ (5) and SLC (11), which allows to examine potential as well as kinetic "pseudo-energy" (originating from the deviations from the desired trajectory).
b) Independent parameterization of contact stiffness and damping gains (in contrast to SLC)
c) The possibility to impose an exponential convergence rate directly by choice of the gains (in contrast to PD+)

The properties as well as some insights about the convergence behavior and concerning the choice of gains are discussed in the following. The control law was first introduced in [6]. A slightly modified[4] version is presented here:

Proposition 1. *Let the control law be*

$$\boldsymbol{\tau}_{\mathrm{GTC}} = \boldsymbol{M}(\boldsymbol{q})\ddot{\boldsymbol{q}}_{\mathrm{ref}} + \boldsymbol{C}(\boldsymbol{q},\dot{\boldsymbol{q}})\dot{\boldsymbol{q}}_{\mathrm{ref}} + \boldsymbol{g}(\boldsymbol{q}) - \boldsymbol{K}\widetilde{\boldsymbol{q}} - \boldsymbol{H}(\boldsymbol{q})\boldsymbol{s}, \quad (12)$$

with the uniformly bounded s.p.d. gain matrix $\boldsymbol{H}(\boldsymbol{q}) \in \mathbb{R}^{n\times n}$ *and the diagonal p.d. gain matrix* $\boldsymbol{K} \in \mathbb{R}^{n\times n}$.

Applying (12) *together with* (7) *and* (8) *to the robot dynamics* (1)*, the equilibrium* $(\widetilde{\boldsymbol{q}}^*, \boldsymbol{s}^*) = (\boldsymbol{0}, \boldsymbol{0})$ *is rendered uniformly exponentially stable for* $\boldsymbol{\tau}_{\mathrm{ext}} = \boldsymbol{0}$.

Proof. Inserting (12), (7) and (8) into (1), the closed-loop equations become

$$\boldsymbol{M}(\widetilde{\boldsymbol{q}},t)\dot{\boldsymbol{s}} + (\boldsymbol{C}(\widetilde{\boldsymbol{q}},\boldsymbol{s},t) + \boldsymbol{H}(\widetilde{\boldsymbol{q}},t))\boldsymbol{s} + \boldsymbol{K}\widetilde{\boldsymbol{q}} = \boldsymbol{\tau}_{\mathrm{ext}} \quad (13)$$

$$\dot{\widetilde{\boldsymbol{q}}} = \boldsymbol{s} - \boldsymbol{\Omega}\widetilde{\boldsymbol{q}}. \quad (14)$$

The following function $V_{\mathrm{GTC}} : \mathcal{Q} \times \mathbb{R}^n \times \mathbb{R}^+ \to \mathbb{R}$ is considered:

$$V_{\mathrm{GTC}}(\widetilde{\boldsymbol{q}},\boldsymbol{s},t) = \frac{1}{2}\boldsymbol{s}^T\boldsymbol{M}(\widetilde{\boldsymbol{q}},t)\boldsymbol{s} + \frac{1}{2}\widetilde{\boldsymbol{q}}^T\boldsymbol{K}\widetilde{\boldsymbol{q}}, \quad (15)$$

which is p.d. in $(\widetilde{\boldsymbol{q}}, \boldsymbol{s})$ for all t. The time derivative of (15) along the trajectories of (13)–(14) is

$$\dot{V}_{\mathrm{GTC}}(\widetilde{\boldsymbol{q}},\boldsymbol{s},t) = \boldsymbol{s}^T\boldsymbol{\tau}_{\mathrm{ext}} - \boldsymbol{s}^T\boldsymbol{H}(\widetilde{\boldsymbol{q}},t)\boldsymbol{s} - \widetilde{\boldsymbol{q}}^T\boldsymbol{K}\boldsymbol{\Omega}\widetilde{\boldsymbol{q}}. \quad (16)$$

Note that $\boldsymbol{K}\boldsymbol{\Omega} \succ \boldsymbol{0}$ due to the definition of $\boldsymbol{K}$ and $\boldsymbol{\Omega}$ as diagonal p.d. matrices. This result immediately shows passivity of (13)-(14) w. r. t. the power port $(\boldsymbol{\tau}_{\mathrm{ext}}, \boldsymbol{s})$.

Furthermore, from (15) and (16) and with (2) follows that $\boldsymbol{q}$ (and thus $\boldsymbol{M}(\boldsymbol{q})$) is bounded. Using the min-max-theorem[5], it is possible to give time-independent bounds for $V_{\mathrm{GTC}}(\widetilde{\boldsymbol{q}},\boldsymbol{s},t)$:

$$\underline{V}_{\mathrm{GTC}}(\widetilde{\boldsymbol{q}},\boldsymbol{s}) = \frac{1}{2}\inf_{\boldsymbol{q}\in\mathcal{Q}}(\min(\lambda(\boldsymbol{M}(\boldsymbol{q}))))\|\boldsymbol{s}\|^2 + \frac{1}{2}\min(\lambda(\boldsymbol{K}))\|\widetilde{\boldsymbol{q}}\|^2 \quad (17)$$

$$\overline{V}_{\mathrm{GTC}}(\widetilde{\boldsymbol{q}},\boldsymbol{s}) = \frac{1}{2}\sup_{\boldsymbol{q}\in\mathcal{Q}}(\max(\lambda(\boldsymbol{M}(\boldsymbol{q}))))\|\boldsymbol{s}\|^2 + \frac{1}{2}\max(\lambda(\boldsymbol{K}))\|\widetilde{\boldsymbol{q}}\|^2 \quad (18)$$

with $\lambda(\cdot)$ denoting the eigenvalues of a matrix. Moreover, for $\boldsymbol{\tau}_{\mathrm{ext}} = \boldsymbol{0}$, (16) is bounded by

$$\dot{\overline{V}}_{\mathrm{GTC}}(\widetilde{\boldsymbol{q}},\boldsymbol{s}) = -\inf_{\boldsymbol{q}\in\mathcal{Q}}(\min(\lambda(\boldsymbol{H}(\boldsymbol{q}))))\|\boldsymbol{s}\|^2 - \min(\lambda(\boldsymbol{K}\boldsymbol{\Omega}))\|\widetilde{\boldsymbol{q}}\|^2, \quad (19)$$

such that

$$\underline{V}_{\mathrm{GTC}}(\widetilde{\boldsymbol{q}},\boldsymbol{s}) \le V_{\mathrm{GTC}}(\widetilde{\boldsymbol{q}},\boldsymbol{s},t) \le \overline{V}_{\mathrm{GTC}}(\widetilde{\boldsymbol{q}},\boldsymbol{s}) \quad (20)$$

and

$$\dot{V}_{\mathrm{GTC}}(\widetilde{\boldsymbol{q}},\boldsymbol{s},t) \le \dot{\overline{V}}_{\mathrm{GTC}}(\widetilde{\boldsymbol{q}},\boldsymbol{s}) < 0 \quad (21)$$

for all $(\widetilde{\boldsymbol{q}}, \boldsymbol{s}) \neq \boldsymbol{0}$. Uniform exponential stability of the origin $(\widetilde{\boldsymbol{q}}^*, \boldsymbol{s}^*) = (\boldsymbol{0}, \boldsymbol{0})$ follows directly from [18, Theorem 4.10, p. 154]. □

Remark 1. The Lyapunov function (15) is radially unbounded for $\boldsymbol{q} \in \mathcal{Q}$. In this sense, the proof of stability holds "globally" for the relevant working space of the robot.

Remark 2. For the sake of completeness, it should be mentioned that the stability properties derived for $(\widetilde{\boldsymbol{q}}, \boldsymbol{s})$ do also apply for the full system error state $(\widetilde{\boldsymbol{q}}, \dot{\widetilde{\boldsymbol{q}}})$, as $\boldsymbol{s}$ can be considered as input of the asymptotically stable $\widetilde{\boldsymbol{q}}$-dynamics (14). Thus, convergence of $\boldsymbol{s}$ directly implies convergence of $\dot{\widetilde{\boldsymbol{q}}}$ (cf. [19, p. 399]).

3.2 Discussion of properties

As mentioned above, the GTC combines components from the PD+ and the SLC. In particular, both of these classical

4 Modification mainly in terms of notation. Also, [6] introduced scalar gains instead of gain matrices.

5 From the Courant-Fischer theorem follows the min-max theorem, which states that $\min(\lambda(\boldsymbol{A}))\|\boldsymbol{z}\|^2 \le \boldsymbol{z}^T\boldsymbol{A}\boldsymbol{z} \le \max(\lambda(\boldsymbol{A}))\|\boldsymbol{z}\|^2$ for a s.p.d. matrix $\boldsymbol{A}$ [17, p. 224-225].

Tab. 1: Effective control gains of the different control laws

control law	$\widetilde{q}$: effective P-gain	$\dot{\widetilde{q}}$: effective D-gain
PD+	$-\boldsymbol{K}$	$-\boldsymbol{D}(\boldsymbol{q})$
SLC	$-\boldsymbol{C}(\boldsymbol{q},\dot{\boldsymbol{q}})\boldsymbol{\Omega}-\boldsymbol{H}(\boldsymbol{q})\boldsymbol{\Omega}$	$-\boldsymbol{M}(\boldsymbol{q})\boldsymbol{\Omega}-\boldsymbol{H}(\boldsymbol{q})$
GTC	$-\boldsymbol{C}(\boldsymbol{q},\dot{\boldsymbol{q}})\boldsymbol{\Omega}-\boldsymbol{H}(\boldsymbol{q})\boldsymbol{\Omega}-\boldsymbol{K}$	$-\boldsymbol{M}(\boldsymbol{q})\boldsymbol{\Omega}-\boldsymbol{H}(\boldsymbol{q})$

control algorithms can be derived as corner cases of the GTC:

- For $\boldsymbol{\Omega}\to\boldsymbol{0}$, (12) becomes a PD+ controller (3).
- For $\boldsymbol{K}\to\boldsymbol{0}$, (12) becomes a Slotine-Li controller (6).

Comparison of control gains: In order to compare the control gains, the SLC and GTC control laws (6) and (12) are written in in the form of the PD+ control law (3), i. e. the "+"-part equals the first three terms of (3), and is contained in all three control laws. The other parts are sorted by $\widetilde{\boldsymbol{q}}$ and $\dot{\widetilde{\boldsymbol{q}}}$. The resulting proportional and derivative gains are denoted as *effective* control gains. They are listed in Table 1.

It can be seen that the SLC as well as the GTC introduce dynamic couplings in the feedback terms. For the SLC, stiffness and damping are coupled via the choice of $\boldsymbol{H}(\boldsymbol{q})$ and $\boldsymbol{\Omega}$. The additional proportional gain $\boldsymbol{K}$ in the GTC allows a "decoupling" of effective stiffness and damping (i. e. you can change the effective stiffness by choosing a suitable $\boldsymbol{K}$ without changing the effective damping). This might be beneficial under certain circumstances, e. g. when intrinsic elastic properties of a system can be used in order to perform a motion more efficiently. In practice, it is possible to implement and tune an SLC, and then add the additional stiffness term $\boldsymbol{K}\widetilde{\boldsymbol{q}}$ in order to adjust or improve convergence and/or compliance behavior.

Stiffness and damping parameterization: An interesting possibility for gain tuning is to look at $\boldsymbol{K}$ as influencing the behavior in physical contact situations. From (13) and (14), it can be verified that the perceived contact stiffness behavior is $(\boldsymbol{H}\boldsymbol{\Omega}+\boldsymbol{K})\widetilde{\boldsymbol{q}}=\boldsymbol{\tau}_{\text{ext}}$ by regarding the static case $\dot{\boldsymbol{q}}=\dot{\boldsymbol{q}}_{\text{des}}=\boldsymbol{0}$ and $\ddot{\boldsymbol{q}}=\ddot{\boldsymbol{q}}_{\text{des}}=\boldsymbol{0}$. This means that with a given choice of $\boldsymbol{H}$ and $\boldsymbol{\Omega}$, it is possible to enforce a desired contact behavior $\boldsymbol{K}_{\text{eff}}\widetilde{\boldsymbol{q}}=\boldsymbol{\tau}_{\text{ext}}$ by setting

$$\boldsymbol{K}=\boldsymbol{K}_{\text{eff}}-\boldsymbol{H}\boldsymbol{\Omega}. \tag{22}$$

However, $\boldsymbol{K}$ must be positive definite to ensure stability with the given Lyapunov function (15). In other words, the perceived contact stiffness for the GTC should be chosen always equal to or larger than $\boldsymbol{H}\boldsymbol{\Omega}$ (which is the perceived contact stiffness of the SLC). In order to overcome this theoretical restriction, another Lyapunov function candidate can be inspected:

$$V^{*}_{\text{GTC}}(\widetilde{\boldsymbol{q}},\boldsymbol{s},t)=\frac{1}{2}\boldsymbol{s}^{T}\boldsymbol{M}\boldsymbol{s}+\frac{1}{2}\widetilde{\boldsymbol{q}}^{T}\boldsymbol{K}\widetilde{\boldsymbol{q}}+\widetilde{\boldsymbol{q}}^{T}\overline{\boldsymbol{H}}\boldsymbol{\Omega}\widetilde{\boldsymbol{q}}, \tag{23}$$

where $\overline{\boldsymbol{H}}$ equals the gain matrix $\boldsymbol{H}$ from (12), which is additionally required to be constant and diagonal. Then, the time derivative w. r. t. (13)-(14) is

$$\dot{V}^{*}_{\text{GTC}}=-\begin{pmatrix}\widetilde{\boldsymbol{q}}\\ \boldsymbol{s}\end{pmatrix}^{T}\begin{pmatrix}\boldsymbol{K}\boldsymbol{\Omega}+2\overline{\boldsymbol{H}}\boldsymbol{\Omega}^{2} & -\overline{\boldsymbol{H}}\boldsymbol{\Omega}\\ -(\overline{\boldsymbol{H}}\boldsymbol{\Omega})^{T} & \overline{\boldsymbol{H}}\end{pmatrix}\begin{pmatrix}\widetilde{\boldsymbol{q}}\\ \boldsymbol{s}\end{pmatrix} \tag{24}$$

which is negative definite if $\overline{\boldsymbol{H}}\succ\boldsymbol{0}$ and

$$\boldsymbol{K}\boldsymbol{\Omega}+2\overline{\boldsymbol{H}}\boldsymbol{\Omega}^{2}-(\overline{\boldsymbol{H}}\boldsymbol{\Omega})^{T}\overline{\boldsymbol{H}}^{-1}\overline{\boldsymbol{H}}\boldsymbol{\Omega}\succ\boldsymbol{0} \tag{25}$$

according to the Schur complement condition [20]. Choosing $\boldsymbol{K}=\gamma\overline{\boldsymbol{H}}\boldsymbol{\Omega}$, it can be verified that

$$(\gamma+1)\overline{\boldsymbol{H}}\boldsymbol{\Omega}^{2}\succ\boldsymbol{0}, \tag{26}$$

which holds for $\gamma>-1$. This shows that the effective stiffness of the GTC can be changed from arbitrarily close to zero up to higher stiffness values compared to the SLC. The effect will be shown in Sec. 4.

Convergence properties: The error dynamics (14) can be regarded as a first-order system in $\widetilde{\boldsymbol{q}}$ with $\boldsymbol{s}$ as input. Thus, through the choice of $\boldsymbol{\Omega}$, it is possible to prescribe the rate of convergence of $\widetilde{\boldsymbol{q}}$. The convergence behavior of the GTC in the error state $\boldsymbol{z}=(\widetilde{\boldsymbol{q}}^{T},\boldsymbol{s}^{T})^{T}$ can be analyzed as a second step. Recalling (19) and (21), it becomes clear that it is possible to directly parameterize the decrease rate of the energy function by choice of the gains $\boldsymbol{H}$ and $\boldsymbol{K}\boldsymbol{\Omega}$. In particular, it is possible to keep the convergence rate of the energy-like function (15) constant by selecting a constant value $\boldsymbol{\Gamma}=\boldsymbol{K}\boldsymbol{\Omega}$. Then, weighting $\boldsymbol{K}$ versus $\boldsymbol{\Omega}$ "shifts" the behavior of the closed-loop system between convergence of the position error within the sliding variable (parametrized by $\boldsymbol{\Omega}$, see (8)) and the parameterization of a desired stiffness (choice of $\boldsymbol{K}$).

A remarkable observation[6] can be made by inspecting the Lyapunov function and its derivative at $\boldsymbol{\tau}_{\text{ext}}=\boldsymbol{0}$: Making the particular choice of gains

$$\boldsymbol{H}(\boldsymbol{q}):=\alpha\boldsymbol{M}(\boldsymbol{q}) \tag{27}$$

$$\boldsymbol{\Omega}:=\alpha\boldsymbol{I} \tag{28}$$

with some constant $\alpha>0$, it can be verified that

$$\dot{V}_{\text{GTC}}=-2\alpha V_{\text{GTC}}. \tag{29}$$

This means that

$$V_{\text{GTC}}(t)=V_{\text{GTC}}(t_0)\,e^{-2\alpha(t-t_0)} \tag{30}$$

With this finding, it is directly possible to conclude exponential decay of the norm of the error states $\boldsymbol{z}$ w. r. t. the matrix

$$\boldsymbol{P}_{\text{e}}=\begin{pmatrix}\boldsymbol{K} & \boldsymbol{0}\\ \boldsymbol{0} & \boldsymbol{M}(\boldsymbol{q})\end{pmatrix}. \tag{31}$$

6 Similar considerations exist for the classical SLC [19, p.409 ff]

Defining $\boldsymbol{z}^T\boldsymbol{P}_\mathrm{e}\boldsymbol{z} = \|\boldsymbol{z}\|_{\boldsymbol{P}_\mathrm{e}}$ leads to

$$\|\boldsymbol{z}(t)\|_{\boldsymbol{P}_\mathrm{e}} = e^{-2\alpha(t-t_0)}\|\boldsymbol{z}(t_0)\|_{\boldsymbol{P}_\mathrm{e}}. \tag{32}$$

In this case, $\|\boldsymbol{z}(t)\|_{\boldsymbol{P}_\mathrm{e}}$ models a "pseudo-energy", originating from the deviations from the desired trajectory[7]. Information about the decay of this energy-like function is directly related to physical properties of the system. Thus, adding the proportional term $\boldsymbol{K}\widetilde{\boldsymbol{q}}$ to the SLC control law (6) can be beneficial in terms of physical meaning of the derived convergence behavior. Note that the considerations above hold independent of $\boldsymbol{K}$. Thus, tuning the GTC boils down to the choice of $\boldsymbol{K}$ while α can be used as a second design parameter specifying the decay rate of the storage function. Here, $\boldsymbol{K}$ can be interpreted as weighting the "potential energy"-like term vs. the "kinetic energy"-like term in (15) and thus, again, as shifting a constant convergence rate between $\widetilde{\boldsymbol{q}}$ and $\boldsymbol{s}$.

Remark 3. For the particular choice (27) and (28), the contact stiffness becomes configuration-dependent: $\boldsymbol{K}_\mathrm{eff} = \alpha^2\boldsymbol{M}(\boldsymbol{q}) + \boldsymbol{K}$. Thus, it is only possible to specify a contact stiffness at a given operating point in this case.

Remark 4. For (27) and (28), the position and velocity error feedback terms in the control law (12) become inertia-dependent. This can be problematic in terms of robustness (see e. g. [3] for a detailed discussion).

Remark 5. Adding a second positive but possibly time-dependent parameter $\boldsymbol{H} := (\alpha + \beta(t))\boldsymbol{M}(\boldsymbol{q})$ with $\boldsymbol{\Omega} := \alpha\boldsymbol{I}$ means adding a negative semi-definite term to the righthand side of (29). Thus, the equality in (30) and (32) becomes a "less or equal". Therefore, the given exponential function becomes an upper bound to describe the real convergence.

3.3 Task-level control for non-redundant robots

The task space is defined by the coordinates $\boldsymbol{x} \in \mathbb{R}^m$ to be computed from the joint space via $\boldsymbol{x} = \boldsymbol{h}(\boldsymbol{q})$. The corresponding velocities can be derived by $\dot{\boldsymbol{x}} = \boldsymbol{J}(\boldsymbol{q})\dot{\boldsymbol{q}}$ with the task Jacobian matrix $\boldsymbol{J}(\boldsymbol{q}) = \partial\boldsymbol{h}(\boldsymbol{q})/\partial\boldsymbol{q}$. The desired (bounded, feasible and time-continuous) task-space trajectory is given by $\boldsymbol{x}_\mathrm{des}(t), \dot{\boldsymbol{x}}_\mathrm{des}(t), \ddot{\boldsymbol{x}}_\mathrm{des}(t)$. The corresponding tracking error is then defined as $\widetilde{\boldsymbol{x}}(t) = \boldsymbol{x} - \boldsymbol{x}_\mathrm{des}(t)$ with the time derivatives $\dot{\widetilde{\boldsymbol{x}}}(t)$ and $\ddot{\widetilde{\boldsymbol{x}}}(t)$. Similar to the joint space, a control law that ensures tracking of a desired trajectory in the task space can be derived by constructing a control law which renders the time-derivative of

$$V_x(\widetilde{\boldsymbol{x}}, \boldsymbol{s}_x, t) = \frac{1}{2}\boldsymbol{s}_x^T\boldsymbol{M}(\widetilde{\boldsymbol{x}}, t)\boldsymbol{s}_x + \frac{1}{2}\widetilde{\boldsymbol{x}}^T\boldsymbol{K}_x\widetilde{\boldsymbol{x}} \tag{33}$$

with a diagonal, p.d. $\boldsymbol{K}_x \in \mathbb{R}^{m\times m}$ negative definite. For non-redundant robots ($m = n$), the mapping $\boldsymbol{x} = \boldsymbol{h}(\boldsymbol{q})$ is 1:1 and locally invertible, thus (33) is positive definite and thus a Lyapunov function for the complete state $(\boldsymbol{q}, \dot{\boldsymbol{q}})$. The resulting control law is derived as

$$\begin{aligned}\boldsymbol{\tau} = \boldsymbol{M}(\boldsymbol{q})\ddot{\boldsymbol{q}}_\mathrm{ref} + \boldsymbol{C}(\boldsymbol{q}, \dot{\boldsymbol{q}})\dot{\boldsymbol{q}}_\mathrm{ref} + \boldsymbol{g}(\boldsymbol{q}) - \\ -\boldsymbol{J}(\boldsymbol{q})^T\boldsymbol{K}_x\widetilde{\boldsymbol{x}} - \boldsymbol{H}_x(\boldsymbol{q})\boldsymbol{s}_x\end{aligned} \tag{34}$$

with $\boldsymbol{H}_x(\boldsymbol{q}) \in \mathbb{R}^{m\times m}$ s.p.d. and the reference trajectory

$$\boldsymbol{J}(\boldsymbol{q})\dot{\boldsymbol{q}}_\mathrm{ref} = \dot{\boldsymbol{x}}_\mathrm{des} - \boldsymbol{\Omega}_x\widetilde{\boldsymbol{x}} \tag{35}$$

with a diagonal p.d. $\boldsymbol{\Omega}_x \in \mathbb{R}^{m\times m}$. Similar to the joint-space case, the sliding variable is defined as

$$\boldsymbol{s}_x = \boldsymbol{J}(\boldsymbol{q})^{-1}(\dot{\widetilde{\boldsymbol{x}}} + \boldsymbol{\Omega}_x\widetilde{\boldsymbol{x}}). \tag{36}$$

Computing the closed-loop dynamics by inserting (34) into (1), the time derivative of (33) becomes

$$\dot{V}_x(\widetilde{\boldsymbol{x}}, \boldsymbol{s}_x, t) = -\boldsymbol{s}_x^T\boldsymbol{H}_x\boldsymbol{s}_x - \widetilde{\boldsymbol{x}}^T\boldsymbol{K}_x\boldsymbol{\Omega}_x\widetilde{\boldsymbol{x}} \tag{37}$$

and is thus negative definite (as long as $\boldsymbol{x}(\boldsymbol{q})$ is locally invertible). This shows uniform local exponential stability[8] of the origin $(\widetilde{\boldsymbol{x}}^*, \boldsymbol{s}_x{}^*) = (\boldsymbol{0}, \boldsymbol{0})$. Using (36), it is also possible to conclude uniform local exponential stability of $(\widetilde{\boldsymbol{x}}^*, \dot{\widetilde{\boldsymbol{x}}}^*) = (\boldsymbol{0}, \boldsymbol{0})$ by verifying that (37) is indeed negative definite also in $(\widetilde{\boldsymbol{x}}, \dot{\widetilde{\boldsymbol{x}}})$.

4 Experimental results

The controller performance in the joint space is validated with experiments on a KUKA LWR IV+ [21], see Fig. 1a. The commercially available robot features 7 revolute joints. The joint torque controllers [22], [23] operate at 3kHz, the outer control loop which is used for implementing the controllers for the experiments is running in 1kHz. A selection of experimental results is also shown in the accompanying video[9].

Experiment 1: Tracking performance In the first experiment, the tracking performance of the GTC is examined. The desired trajectory for all seven joints of the

7 The above considerations do also hold for $\boldsymbol{z}_e = (\widetilde{\boldsymbol{q}}, \dot{\widetilde{\boldsymbol{q}}})$.

8 Note that it is in general not possible to show task-space stability globally due to singularities or tasks defined in SE(3).

9 The video is available under https://www.youtube.com/watch?v=rQcEfocGjVY.

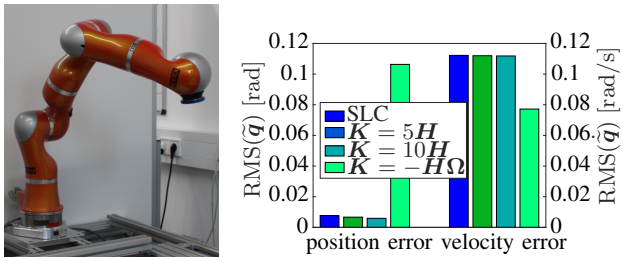

(a) (b)

Fig. 1: a) The KUKA LWR IV+ in its initial pose for the tracking experiments 1 and 2, described in Sec. 4.
b) Comparison of joint position and velocity errors for different stiffness parameterizations (cf. Experiment 1, undisturbed trajectory tracking).

LWR is shown in the upper plot of Fig. 2. As a baseline, an SLC is implemented and the gains are manually tuned to reach decent tracking performance[10]. The resulting gains are $\boldsymbol{\Omega} = \mathrm{diag}(30, 30, 30, 30, 30, 30, 30, 30)\frac{1}{\mathrm{s}}$ and $\boldsymbol{H} = \mathrm{diag}(50, 50, 50, 20, 10, 5, 5)\frac{\mathrm{Nms}}{\mathrm{rad}}$. The value of $\boldsymbol{K}$ is set to different values in order to compare the tracking performance. Thereby, $\boldsymbol{K}$ is chosen proportional to $\boldsymbol{H}$ in order to incorporate the different load and motor characteristics of the single joints.

The tracking performance is displayed in the plots b) and c) of Fig. 2, which shows the Euclidean norm of the position and velocity errors. As expected, the position error decreases with higher values of $\boldsymbol{K}$, whereas the velocity error remains unchanged. In fact, adding a positive $\boldsymbol{K}\widetilde{\boldsymbol{q}}$ to the control law means increasing the stiffness on a given SLC implementation, while leaving the the effective D-gain unchanged (cf. Table 1). In Fig. 1b, the root mean square (RMS) of the position and velocity errors are depicted. Here, an additional parameterization was added to the comparison: adding a negative $\boldsymbol{K}\widetilde{\boldsymbol{q}}$ in order to reduce the effective P-gain. It turned out that choosing $\boldsymbol{K}$ negative up to $\boldsymbol{K} = -\boldsymbol{H}\boldsymbol{\Omega}$ yields a stable behavior, where the perceived stiffness $\boldsymbol{K}_{\mathrm{eff}}$ of the SLC controller is reduced until $\boldsymbol{K}_{\mathrm{eff}} = \boldsymbol{0}$. One can see that in this case, the position error is significantly higher than for the positive effective stiffness values, but in contrast, the velocity error is lower. This shows that in fact, with the GTC it is possible chose the effective P-gain and effective D-gain completely independent. Moreover, it is possible to assign an arbitrary contact stiffness to a given SLC implementation.

10 A comparison of the tracking performance to the PD+ controller is not considered to be meaningful, as the effective P- and D-gains are configuration-dependent for SLC and GTC, cf. Table 1.

Experiment 2: Tracking with external torques For the second experiment, the same trajectory as in Exp. 1 is commanded. In order to investigate the effect of disturbances on the tracking performance, virtual external torques of ±20Nm are applied at the first three joints between $t = 1\mathrm{s}$ and $t = 3\mathrm{s}$, see Fig. 3 a). The tracking results for two parameterizations are shown in plots b) and c). Another question investigated with this experiment is how good the theoretically computed contact stiffness would be perceived in a contact situation with the robot moving on a trajectory. This can be estimated comparing the measured joint deflections caused by the virtual external torques to the expected joint deflections which are computed for the static case as $\widetilde{\boldsymbol{q}}_{\mathrm{comp.}} = \boldsymbol{K}_{\mathrm{eff}}^{-1}\boldsymbol{\tau}_{\mathrm{ext,virt}}$. Plot d) shows the achieved joint stiffness for joint 2 exemplarily. The dashed lines denote the computed joint deflections, the other lines are the measured joint position errors. Deviations originate among other things from the Coriolis terms in the effective P-gain (cf. Table 1), which is present during the execution of a trajectory. Still, it is visible that the measured joint deflections fit the stiffness parameterization.

Experiment 3: Physical interaction The third experiment considers physical interaction with a human operator. Thereby, the robot is commanded to maintain a constant configuration, which can be inspected in Fig. 4. The external torques exerted on the robot are estimated by using the momentum-based observer from [24, 25]. The observer gain is chosen as $25\frac{1}{\mathrm{s}}$. For the interaction, the parameter $\boldsymbol{H}$ is reduced to $\boldsymbol{H} = \mathrm{diag}(15, 15, 15, 6, 3, 1.5, 1.5)\frac{\mathrm{Nms}}{\mathrm{rad}}$ in order to investigate the effect of the perceived stiffness. $\boldsymbol{K}$ was chosen as $\boldsymbol{K} = -\boldsymbol{\Omega}\boldsymbol{H}$, $\boldsymbol{K} = 0\frac{1}{\mathrm{s}}\boldsymbol{H}$ (which is equal to the SLC), and $\boldsymbol{K} = 100\frac{1}{\mathrm{s}}\boldsymbol{H}$, respectively. It could be observed, that the GTC is stable with all chosen gains, even with very high perceived stiffness $\boldsymbol{K}_{\mathrm{eff}} = \boldsymbol{K} + \boldsymbol{H}\boldsymbol{\Omega} = \mathrm{diag}(1950, 1950, 1950, 780, 390, 195, 195)\frac{\mathrm{Nm}}{\mathrm{rad}}$ and zero perceived stiffness at $\boldsymbol{K} = -\boldsymbol{H}\boldsymbol{\Omega}$. The stability and the contact behavior can be verified exemplarily for three choices of $\boldsymbol{K}$ in Fig. 5 and Fig. 6. In Fig. 5, the SLC is compared to a GTC with $\boldsymbol{K} = 100\frac{1}{\mathrm{s}}\boldsymbol{H}$. In the upper plots, the manually applied external torques are plotted, the joint errors are shown in the lower plots. It is visible that the external torques are in the same order of magnitude, while the corresponding joint errors are smaller and converge faster for the higher stiffness. In Fig. 6, the behavior of the GTC with $\boldsymbol{K} = -\boldsymbol{H}\boldsymbol{\Omega}$ is depicted. It can be observed that application of external torques leads to remaining deviations in the joints. Summarized, the interaction experiments verify both stability and the theoretically resulting perceived stiffness of the GTC, in both extreme configurations and extreme parameterizations.

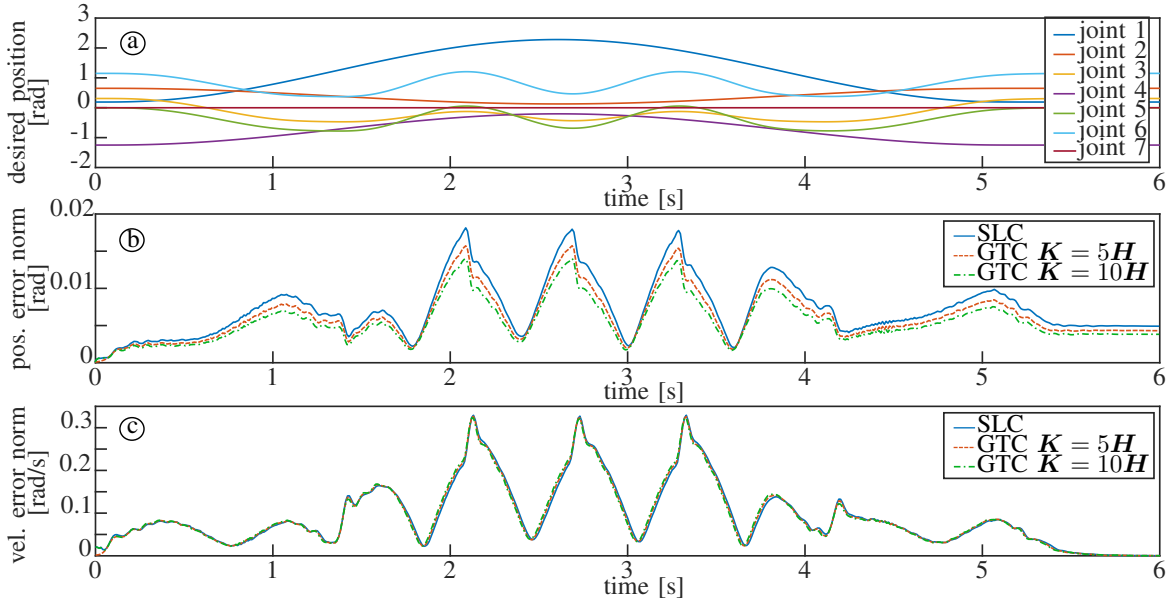

Fig. 2: Experiment 1, undisturbed trajectory. The gains are chosen as $\boldsymbol{\Omega} = \mathrm{diag}(30, 30, 30, 30, 30, 30, 30, 30)\frac{1}{\mathrm{s}}$ and $\boldsymbol{H} = \mathrm{diag}(50, 50, 50, 20, 10, 5, 5)\frac{\mathrm{Nms}}{\mathrm{rad}}$. Plot a): Desired trajectory in joint space. Plot b): RMS of joint position errors for different values of $\boldsymbol{K}$. Plot c): RMS of joint velocity errors for different values of $\boldsymbol{K}$. It is visible that the RMS of the joint position errors changes due to the increased effective stiffness, whereas the RMS of the joint velocity errors remain unchanged.

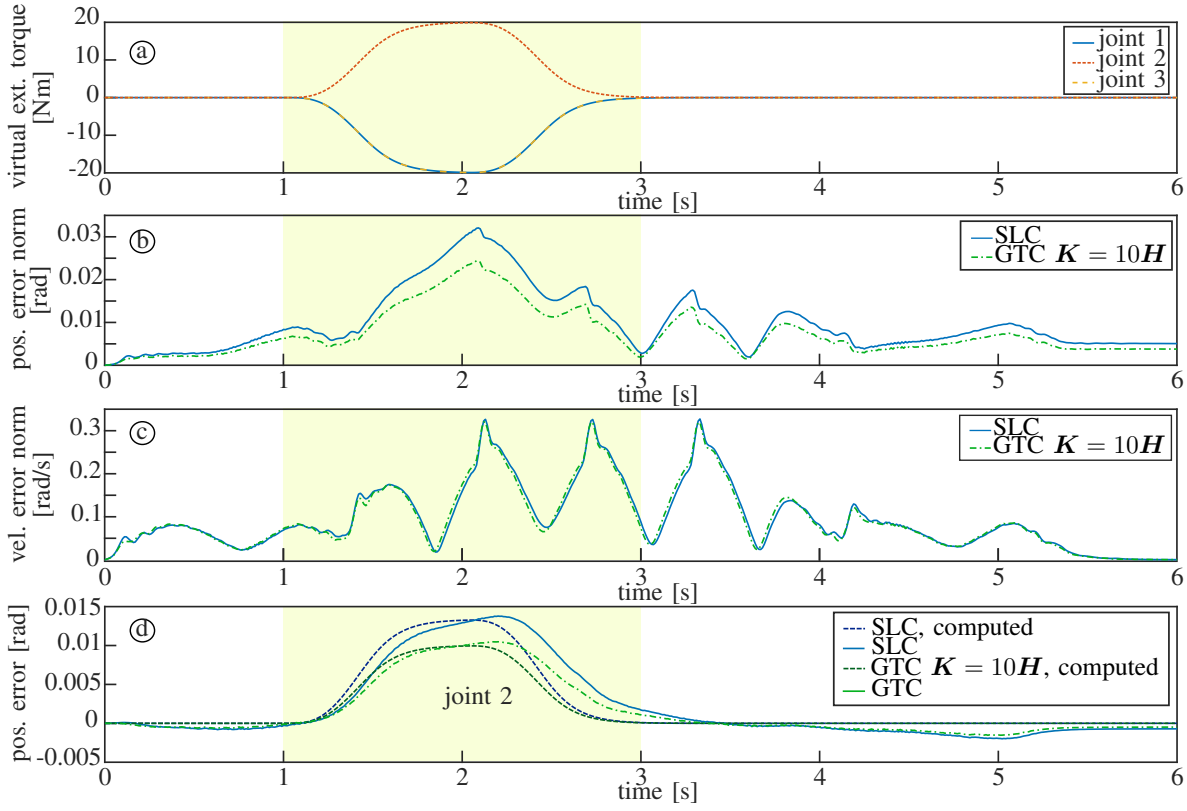

Fig. 3: Experiment 2, trajectory with virtual external torques, the gains were chosen as in Exp. 1. Plot a): Virtual external torques applied to the first three joints. Plot b): RMS of joint position errors for the GTC compared to the SLC. Plot c): RMS of joint velocity errors for the GTC compared to the SLC. Plot d): Measured joint position deviation of joint 2 vs. computed joint position error. The error was computed for the static case as $\widetilde{\boldsymbol{q}}_{\mathrm{comp.}} = \boldsymbol{K}_{\mathrm{eff}}^{-1}\boldsymbol{\tau}_{\mathrm{ext,virt}}$.

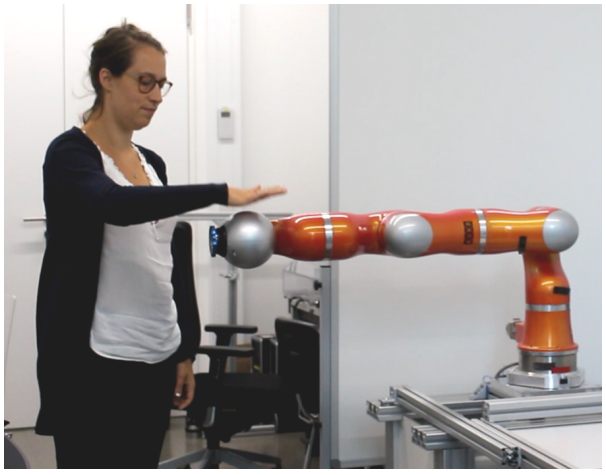

Fig. 4: Initial robot pose for the interaction experiments: $\boldsymbol{q} = (-\pi/2, \pi/2, 0, 0, 0, 0, 0)\text{rad}$.

5 Discussion

Experimental setup: The robot dynamics are considered to be rigid (1), even though the joints of the LWR are in fact elastic. Due to the high joint stiffness (around 10k to 20k $\frac{\text{Nm}}{\text{rad}}$), the link-side dynamics of LWRs can be treated separately from the motor dynamics through the singular perturbation assumption [26]. This property is exploited in the low-level joint torque controllers [22], [23], which justifies the assumption of a rigid body dynamics.

Applicability and future work: The GTC algorithm can be used for trajectory tracking of robotic arms in the joint space, an extension to the task space is possible as proposed in Sec. 3.3. Regarding the implementation, the GTC is not expensive. In fact, adding a position feedback term to an SLC-implementation is sufficient. As pointed out in Sec. 3.2, it is then possible to create both a PD+ controller and an SLC as corner cases by proper selection of the respective gains. From this insight, different possible gain tuning strategies arise. One of several possibilities is experimentally examined in Sec. 4, where an existing SLC implementation is used as a baseline w. r. t. the trajectory tracking behavior. The additional P-gain is then used to adjust the stiffness according to the task (either tracking or interaction). Remarkably, it could be shown that the effective stiffness can be reduced compared to the SLC while maintaining the full velocity tracking performance. If the model is sufficiently good (or the controller is used together with a parameter adaption part, see below), this creates the possibility to create a high tracking performance, while the contact stiffness is still low. This property predestines the GTC among others to human-robot interaction scenarios. On the other hand, increasing the effective stiffness w. r. t. the SLC creates the possibility to create underdamped closed-loop behavior, opening the door for control strategies which exploit the inherent elasticity of the hardware in order to increase efficiency.

Last, it is worth mentioning that it is possible to extend the GTC with a parameter adaption part as in [6]. Similarly, a parameter adaption for the original SLC is proposed in [5]. The adaption part is able to increase the robustness w. r. t. parameter uncertainties.

6 Conclusion

In this work, a passivity-based control approach for the trajectory tracking of robotic arms was analyzed. The theoretical and practical knowledge about the *Generalized Robot Tracking Controller* has significantly been extended and experimentally verified using a commercially available robot arm. The advantages of the control approach in contrast to the well-known PD+ and Slotine-Li tracking controllers were demonstrated and discussed.

References

[1] E. Freund, "Fast Nonlinear Control with Arbitrary Pole-Placement for Industrial Robots and Manipulators," *The International Journal of Robotics Research*, vol. 1, no. 1, pp. 65–78, Mar. 1982.

[2] M. Spong and M. Vidyasagar, "Robust nonlinear control of robot manipulators," in *1985 24th IEEE Conference on Decision and Control*. Fort Lauderdale, FL, USA: IEEE, Dec. 1985, pp. 1767–1772.

[3] A. Dietrich, X. Wu, K. Bussmann, M. Harder, M. Iskandar, J. Englsberger, C. Ott, and A. Albu-Schäffer, "Practical consequences of inertia shaping for interaction and tracking in robot control," *Control Engineering Practice*, vol. 114, p. 104875, Sep. 2021.

[4] B. Paden and R. Panja, "Globally asymptotically stable 'PD+' controller for robot manipulators," *International Journal of Control*, vol. 47, no. 6, pp. 1697–1712, Jun. 1988, publisher: Taylor & Francis.

[5] J.-J. E. Slotine and W. Li, "On the Adaptive Control of Robot Manipulators," *The International Journal of Robotics Research*, vol. 6, no. 3, pp. 49–59, Sep. 1987.

[6] N. Sadegh and R. Horowitz, "Stability and Robustness Analysis of a Class of Adaptive Controllers for Robotic Manipulators," *The International Journal*

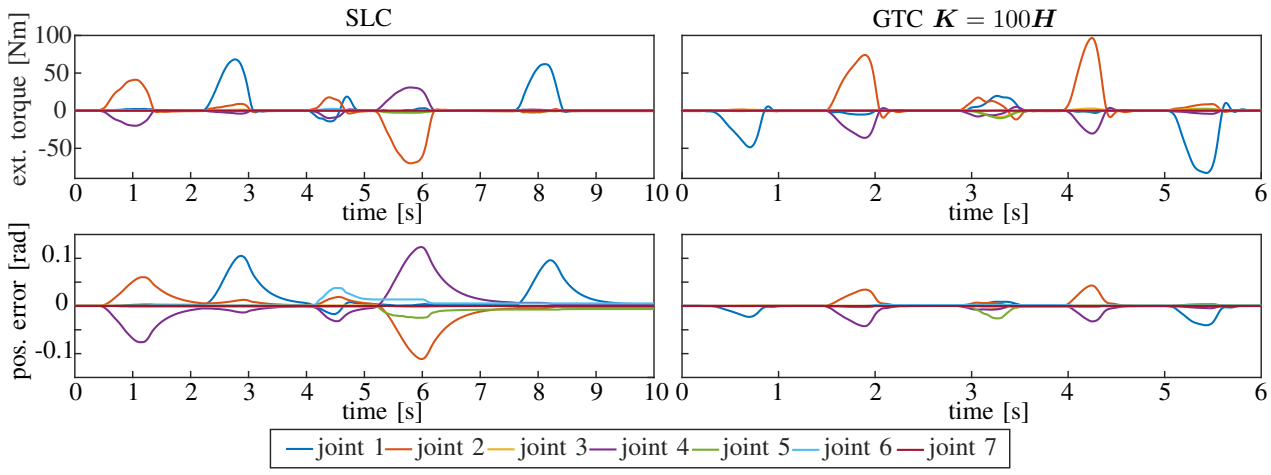

Fig. 5: Experiment 3: physical interaction. Left plot: SLC implementation with $\boldsymbol{\Omega} = \mathrm{diag}(30, 30, 30, 30, 30, 30, 30, 30)\frac{1}{\mathrm{s}}$, $\boldsymbol{H} = \mathrm{diag}(15, 15, 15, 6, 3, 1.5, 1.5)\frac{\mathrm{Nms}}{\mathrm{rad}}$. Right plot: GTC with increased effective stiffness.

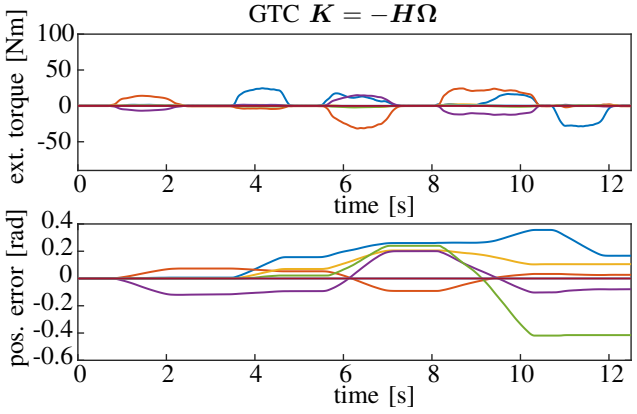

Fig. 6: Experiment 2: Physical interaction. GTC implementation with zero perceived stiffness.

of Robotics Research, vol. 9, no. 3, pp. 74–92, Jun. 1990.

[7] T. Hatanaka, N. Chopra, and M. W. Spong, "Passivity-based control of robots: Historical perspective and contemporary issues," in *2015 54th IEEE Conference on Decision and Control (CDC)*, Dec. 2015, pp. 2450–2452.

[8] M. W. Spong, "An Historical Perspective on the Control of Robotic Manipulators," *Annual Review of Control, Robotics, and Autonomous Systems*, vol. 5, no. 1, pp. 1–31, May 2022.

[9] J.-J. E. Slotine and W. Li, "Adaptive manipulator control: A case study," *IEEE Transactions on Automatic Control*, vol. 33, no. 11, pp. 995–1003, Nov. 1988.

[10] R. Ortega and M. Spong, "Adaptive motion control of rigid robots: A tutorial," in *Proceedings of the 27th IEEE Conference on Decision and Control*, Dec. 1988, pp. 1575–1584 vol.2.

[11] H. Berghuis and H. Nijmeijer, "A passivity approach to controller-observer design for robots," *IEEE Transactions on Robotics and Automation*, vol. 9, no. 6, pp. 740–754, Dec. 1993.

[12] J. M. A. Scherpen and R. Ortega, "On nonlinear control of Euler-Lagrange systems: Disturbance attenuation properties," *Systems & Control Letters*, vol. 30, no. 1, pp. 49–56, Mar. 1997.

[13] C. Ren, Y. Ding, and S. Ma, "Passivity-Based Active Disturbance Rejection Control of an Omnidirectional Mobile Robot," in *2018 IEEE 8th Annual International Conference on CYBER Technology in Automation, Control, and Intelligent Systems (CYBER)*, Jul. 2018, pp. 1513–1518.

[14] R. M. Murray, Z. Li, and S. S. Sastry, *A Mathematical Introduction to Robotic Manipulation*, 1st ed. CRC Press, 1994.

[15] F. Ghorbel, B. Srinivasan, and M. W. Spong, "On the uniform boundedness of the inertia matrix of serial robot manipulators," *Journal of Robotic Systems*, vol. 15, no. 1, pp. 17–28, 1998.

[16] M. Spong, R. Ortega, and R. Kelly, "Comments on 'Adaptive manipulator control: a case study' by J. Slotine and W. Li," *IEEE Transactions on Automatic Control*, vol. 35, no. 6, pp. 761–762, 1990.

[17] H. Dym, *Linear Algebra in Action: Second Edition*. American Mathematical Soc., Dec. 2013, vol. 78.

[18] H. K. Khalil, *Nonlinear Systems*, 3rd ed. Upper Saddle River, NJ: Prentice Hall, 2002.

[19] J.-J. E. Slotine and W. Li, *Applied Nonlinear Control*. Englewood Cliffs, NJ: Prentice Hall, 1991.

[20] F. Zhang, Ed., *The Schur Complement and Its Applications*, ser. Numerical Methods and Algorithms. New York: Springer Science and Business Media, 2005, no. 4.

[21] R. Bischoff, J. Kurth, G. Schreiber, R. Koeppe, A. Albu-Schäffer, A. Beyer, O. Eiberger, S. Haddadin, A. Stemmer, G. Grunwald, and G. Hirzinger, "The KUKA-DLR lightweight robot arm - a new reference platform for robotics research and manufacturing," in *ISR 2010 (41st International Symposium on Robotics) and ROBOTIK 2010 (6th German Conference on Robotics)*, 2010, pp. 1–8.

[22] A. Albu-Schäffer, C. Ott, and G. Hirzinger, "A Unified Passivity-based Control Framework for Position, Torque and Impedance Control of Flexible Joint Robots," *International Journal of Robotics Research*, vol. 27, no. 1, pp. 23–39, Jan. 2007.

[23] C. Ott, A. Albu-Schäffer, A. Kugi, and G. Hirzinger, "On the Passivity-Based Impedance Control of Flexible Joint Robots," *IEEE Transactions on Robotics*, vol. 24, no. 2, pp. 416–429, Apr. 2008.

[24] A. De Luca, A. Albu-Schäffer, S. Haddadin, and G. Hirzinger, "Collision detection and safe reaction with the DLR-III lightweight manipulator arm," in *IEEE/RSJ International Conference on Intelligent Robots and Systems*, Oct. 2006, pp. 1623–1630.

[25] S. Haddadin, A. De Luca, and A. Albu-Schäffer, "Robot collisions: A survey on detection, isolation, and identification," *IEEE Transactions on Robotics*, vol. 33, no. 6, pp. 1292–1312, Dec. 2017.

[26] C. Ott, *Cartesian Impedance Control of Redundant and Flexible-Joint Robots*, ser. Springer Tracts in Advanced Robotics. Springer Publishing Company, Berlin Heidelberg, 2008, vol. 49.

Bionotes

Kristin Lakatos received her M.Sc. degree in mechanical engineering with focus on control theory and information technology from the Technical University of Munich (TUM) in 2014. In the same year, she joined the German Aerospace Center (DLR), Institute of Robotics and Mechatronics, as a research assistant. Her current research interests include passivity-based control concepts, the control of nonholonomic systems and mobile manipulation.

Dominic Lakatos received the Dipl.-Ing. degree in mechanical engineering from the University of Applied Sciences Munich, Germany, in 2011, and the PhD in theoretical mechanics, robotics and control theory from the Technical University of Munich, Germany, in 2018. From 2011 to 2019, he has been with the Institute of Robotics and Mechatronics, German Aerospace Center, Wessling, Germany, as a research associate. From 2017 to 2023, he has been with the lidar company Blickfeld GmbH, Munich, Germany, heading and developing MEMS scanner control, and since 2023 he is with Carl Zeiss SMT, Oberkochen, Germany, as Cluster Architect for System Control of EUV Lithography Optics. His main research interests include control of nonlinear systems, underactuated systems, human and robotic dynamics, nonlinear oscillations, limit cycles, robot design, bioinspired and legged robots, control systems, MEMS design and control, optics, and EUV lithography optics.

Xuwei Wu received the B.E. degree in vehicle engineering from the Tongji University, Shanghai, China, in 2013, and the M.Sc. degree in mechanical engineering from the Technical University of Munich (TUM), Germany, in 2016. In 2019, he joined the German Aerospace Center (DLR), Institute of Robotics and Mechatronics, as a research assistant. His current research interests include nonlinear stability theory, whole-body control of humanoid robots, and safe physical human-robot interaction.

Paul Kotyczka received the Dipl.-Ing. degree in Electrical Engineering and the Dr.-Ing. degree in Automatic Control from Technical University of Munich (TUM) in 2005 and 2010, respectively. From 2015 to 2017 he was a Marie Skłodowska-Curie Fellow at the Laboratory of Automatic Control, Chemical and Pharmaceutical Engineering (LAGEPP), University Claude Bernard Lyon 1. After his habilitation in 2019 he became Privatdozent (adjunct teaching professor). He leads the Energy-based Modeling and Control Group at the Chair of Automatic Control, TUM. He works on structured modeling, geometric numerical methods and nonlinear control design for multi-domain physical systems, with applications to mechatronic, robotic and process systems. He is program coordinator of the French-German Doctoral College Port-Hamiltonian Systems: Modeling, Numerics and Control.

Alexander Dietrich received the Dr.-Ing. degree from the Technical University of Munich (TUM) in 2015. In 2010, he joined the German Aerospace Center (DLR), Institute of Robotics and Mechatronics, as a research scientist. Among others, he received the Georges Giralt PhD Award 2016 for the best European thesis in robotics, the DLR Science Award in 2020, and the Distinguished Service Award for Outstanding Associate Editors of the IEEE Robotics and Automation Letters in 2020. He published more than 60 peer-reviewed papers in international journals, books and on conferences, and he is holding 13 patents. He is IEEE Senior Member, Editor of the IEEE ICRA (2020-2022), Associate Editor for IEEE T-RO (since 2021), IEEE RA-M (2018-2020), IEEE RA-L (2017-2021), and he was co-chair of the IEEE RAS Technical Committee on Whole-Body Control (2018-2021). Since 2017 he is head of the whole-body control group at the Institute of Robotics and Mechatronics of the DLR, and since 2019 he is lecturer at TUM on the control of modern lightweight robots. His current research interests include whole-body mobile manipulation, impedance and force control, hierarchical control for kinematically redundant robots, safe physical human–robot interaction, and the stability analysis of the corresponding control approaches.